ACS APPLIED MATERIALS & INTERFACES

Research Article

www.acsami.org

Dibenzopyran-Based Wide Band Gap Conjugated Copolymers: Structural Design and Application for Polymer Solar Cells

Yuanyuan Zhou,[†] Miao Li,[†] Yijing Guo,[†] Heng Lu,[‡] Jinsheng Song,*[,†] Zhishan Bo,*[,‡] and Hua Wang*[,†]

[†]Engineering Research Center for Nanomaterials, Henan University, Kaifeng, 475004, China

[‡]Beijing Key Laboratory of Energy Conversion and Storage Materials, College of Chemistry, Beijing Normal University, Beijing 100875, China

Supporting Information

ABSTRACT: With the efficient synthesis of the crucial dibenzopyran building block, a series of **PDBPTBT** polymers containing different alkyl side chains and/or fluorine substitution were designed and synthesized via the microwave-assisted Suzuki polycondensation. Quantum chemistry calculations based on density functional theory indicated that different substitutions have significant impacts on the planarity and rigidity of the polymer backbones. Interestingly, the alkyloxy chains of **PDBPTBT-4** tend to stay in the same plane with the benzothiadiazole unit, but the others appear to be out of plane. With the S···O and F···H/F···S supramolecular interactions, the conformations of the four polymers will be locked in different ways as predicted by the quantum chemistry calculation. Such structural variation resulted in varied solid stacking and photophysical properties as well as the final photovoltaic performances. Conventional devices based on these four polymers were fabricated, and **PDBPTBT-5** displayed the best PCE of 5.32%. After optimization of the additive types, ratios, and the interlayers at the cathode, a high PCE of 7.06% (V_{oc} = 0.96 V, J_{sc} = 11.09 mA/cm^2, and FF = 0.67) is obtained for **PDBPTBT-5** with 2.0% DIO as the additive and PFN-OX as the electron-transporting layer. These results indicated DBP-based conjugated polymers are promising wide band gap polymer donors for high-efficiency polymer solar cells.

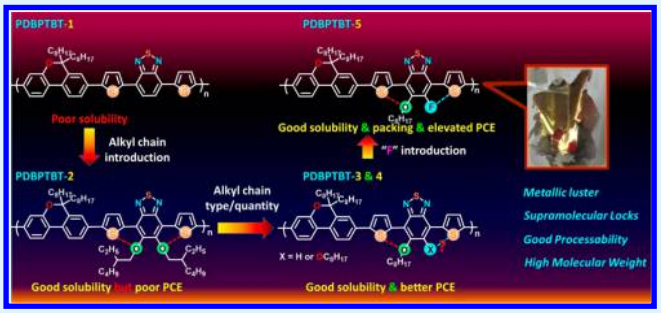

KEYWORDS: *dibenzopyran, wide band gap, supramolecular interaction, polymer solar cells, electron-transporting layer, quantum chemistry calculations*

INTRODUCTION

Polymer solar cells (PSCs) have attracted more and more attention due to their advantages such as relatively high efficiency, easy fabrication, low fabrication cost, and lightweight in comparison with their inorganic counterpart. Great effort has been devoted to modulating the properties of active layers, which have strongly advanced the development of this field in the past decade, and recently, power conversion efficiencies (PCEs) have achieved over 10% for both single junction and multijunction tandem PSCs.[1] Generally, wide and low band gap materials are used for the front and rear cells, respectively, to improve the light-harvesting ability of tandem cells. Although remarkable progress has been achieved for low band gap π-conjugated copolymers with an alternating donor−acceptor (D−A) structure, the development of wide band gap still lags behind. In this regard, designing and synthesizing new wide band gap conjugated polymers with high V_{oc} and respectable photovoltaic performance are extremely important and desirable for developing tandem solar cells with high efficiencies.[2−4]

Pyran is a six-membered heterocyclic ring, consisting of five carbon atoms, one oxygen atom, and two double bonds. There are two isomers for pyran that differ by the location of the double bonds as shown in Chart 1. 4*H*-Pyran, whose saturated carbon is at position 4, has been widely used in dye-sensitized solar cells,[5] fluorescence probe,[6] nonlinear optical chromophores,[7] organic light-emitting diode,[8] and so on, and the basic structures are depicted in Chart 1. However, in 2*H*-pyran, the saturated carbon is located at position 2, and the well-known chemical structures comprising the 2*H*-pyran segments are coumarin and spiropyran as shown in Chart 1, which have been widely used as fluorescent chromophore in ion detection,[9] protein phototrigger,[10] super-resolution imaging,[11] and so on.

Recently, Yang et al. reported a new donor 5*H*-dithieno[3,2-b:2′,3′-d]pyran (DTP), which annulated the 2,2′-bithiophene with 2*H*-pyran.[1,12] By using this novel unit as the electron-donating block for the D−A polymer, a high PCE of 10% was achieved for polymer solar cell devices. Very recently, Jo et al.[13] and our group[14] have separately reported a dibenzopyran (DBP) building block for PSCs, which also includes a 2*H*-pyran segment and could be efficiently synthesized with our simple method. The preliminary results indicated that the **PDBPTBT**

Received: September 7, 2016
Accepted: October 24, 2016
Published: October 24, 2016

DOI: 10.1021/acsami.6b11348
ACS Appl. Mater. Interfaces 2016, 8, 31348−31358

Chart 1. Examples of Pyran-Based Fragments Utilized in Literature

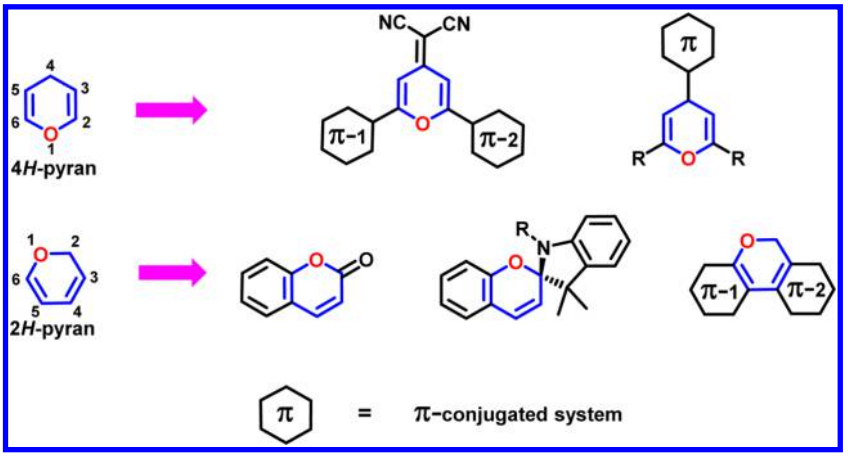

Chart 2. Designing Concept and Chemical Structures of the DBP-Based Conjugated Polymers Used for PSCs

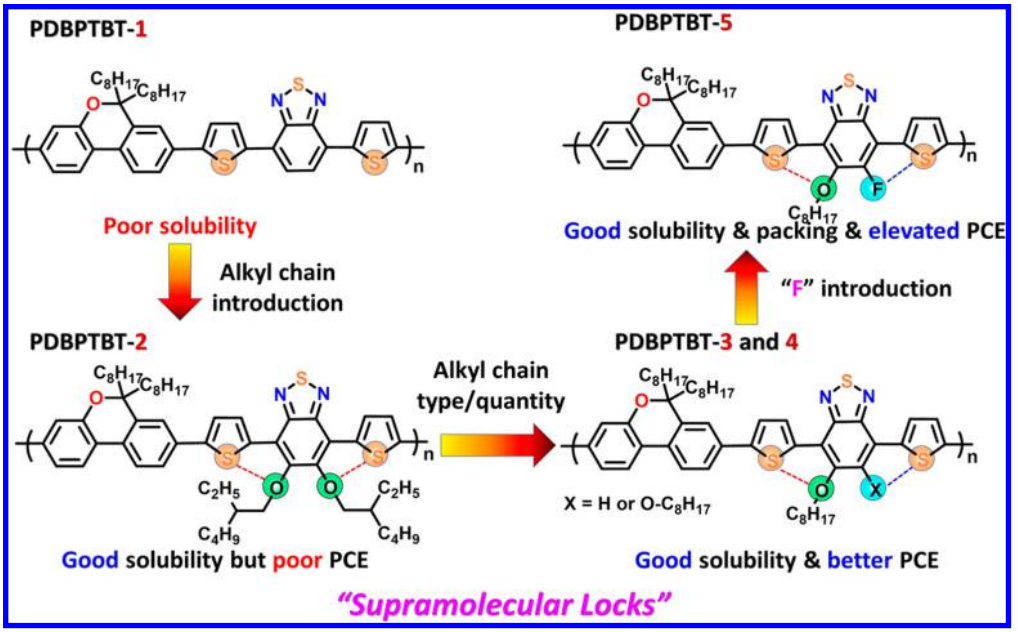

polymers are of great potential for high-efficiency polymer solar cells, though the solubility of **PDBPTBT-1** is poor in common organic solvents.

As we all know, the molecular weight of conjugated polymers plays a pivotal role in the performance of devices, and it will be influenced by the solubility of polymer, types of the side chain, planarity of the main-chains, and so on. To achieve high-performance polymer donor materials, careful design of the side chain and substituted group is required to balance the solubility and main chain packing of the final polymers.[15] As shown in Chart 2, **PDBPTBT-1** presents a moderate PCE of 2.88%, but poor solubility.[14] However, by introducing two branched ethylhexyloxy side chains to the benzothiadiazole (BT) unit, the solubility of **PDBPTBT-2** (M_n = 10.5 kg/mol) was improved, but poorer photovoltaic performance (PCE = 2.20%) was obtained. So, in this manuscript, we focus on the structural design and synthesis of DBP-based conjugated polymers for high efficiency PSCs via modification of the side chains and substituted groups. First, microwave-assisted Suzuki polycondensation was tried for the synthesis of **PDBPTBT-2** in order to achieve higher molecular weight polymers. The molecular weight increased from 10.5 kg/mol by conventional heating[14] to 51.4 kg/mol by the microwave-assisted polymerization, PSCs based on high molecular weight **PDBPTBT-2** gave an elevated PCE of 3.28%. According to the current achievements and developing trend of donor polymers in polymer photovoltaics, it appears to be significantly important that structural conformation must be taken into consideration during the polymer backbone design and optimization.[16] In this work, we designed some new DBP-based polymers via introducing different substituted groups and initially tried to utilize the theoretical calculation to predict the conformational properties of these conjugated polymers and then systematically studied the structure–property relationship. Since the efficient microwave-assisted polymerization method displayed the advantage versus the traditional heating during the **PDBPTBT-2** preparation, it was applied for the other DBP polymer preparation. As depicted in Chart 2, if the DBP monomer was polymerized with BT monomers with one or two linear octyloxy chains, the final polymers continued to maintain the good solubility and a better PCE of up to 4.24% was obtained by the single octyloxy chain modified **PDBPTBT-4**. Finally, monofluoro-substituted benzothiadiazole was incorporated into the main chain, and a PCE of 7.06% was

DOI: 10.1021/acsami.6b11348
ACS Appl. Mater. Interfaces 2016, 8, 31348–31358

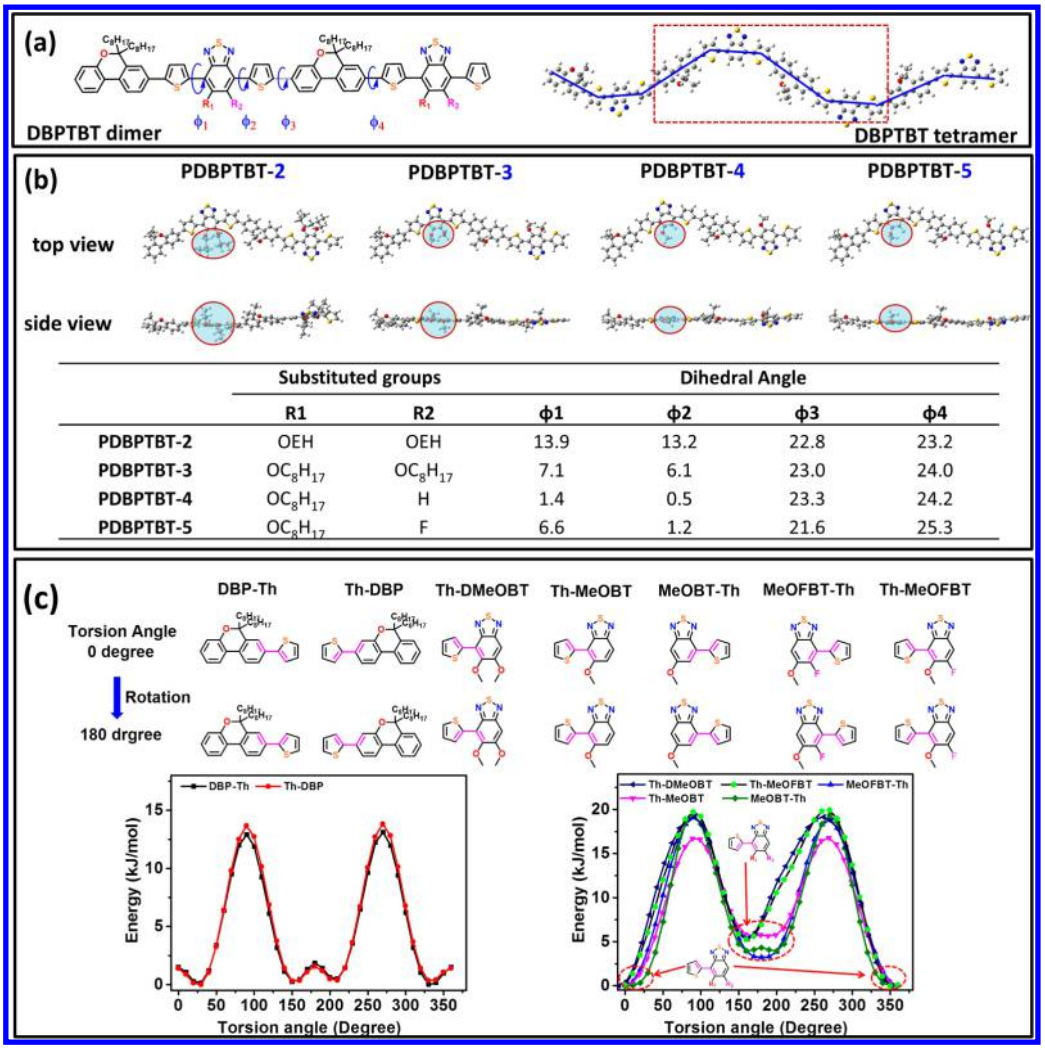

	Substituted groups		Dihedral Angle			
	R1	R2	ϕ1	ϕ2	ϕ3	ϕ4
PDBPTBT-2	OEH	OEH	13.9	13.2	22.8	23.2
PDBPTBT-3	OC_8H_{17}	OC_8H_{17}	7.1	6.1	23.0	24.0
PDBPTBT-4	OC_8H_{17}	H	1.4	0.5	23.3	24.2
PDBPTBT-5	OC_8H_{17}	F	6.6	1.2	21.6	25.3

Figure 1. (a) Representative example of the DBPTBT tetramer and the typical dihedral angles in the dimer; (b) DFT-optimized conformations and dihedral angles in the dimers of the **PDBPTBT** polymers; (c) potential energy surface scan of the of the possible rotamers in the four polymers.

achieved after the introduction of a thin PFN-OX layer, which is higher than the other wide band gap polymers based on the dibenzene building blocks (fluorene, dibenzosilole, dibenzothiophene, and carbazole) and BT derivatives.[17−20] This improvement might be ascribed to the formation of a more straight and planar main chain of **PDBPTBT-5**, which was possibly initiated by the supramolecular conformation locks of S···O[18,21,22] and F···H[23]/ F···S[24,25] confirmed by DFT quantum chemistry calculation and XRD results.

RESULTS AND DISCUSSION

Considerations for Chemical Structures by Quantum Calculations. Considering the potential usage of the novel DBP moiety for high-efficiency wide band gap polymers in organic photovoltaics, a series of new DBP-based polymers have been designed via the careful selection of the alkyloxy chains and substituted groups on the comonomers. The optimized geometries of model compounds under the ground state were calculated from density functional theory (DFT) at B3LYP/6-31G(d,p) level using the Gaussian 09 package.

As shown in Figure 1a, the theoretical calculation result for the tetramer of **PDBPTBT-1** polymer reveals that the optimal geometry of the conjugated backbone bears a zigzagged conformation.[14] To simplify the calculation processes and compare the configurations of the main chain influenced by the substituted groups, the dimers of these **PDBPTBT** polymer have been constructed and optimized with theoretical calculation employing the DFT with the B3LYP/6-31G (d,p) basis set. The alkyls are simplified to methyl groups as shown in Figure 1b, and the dihedral angles (φ_1, φ_2, φ_3, and φ_4) are depicted as Figure 1a. It is interesting that all dimers bearing the zigzagged conjugated backbones present similar top views, but the specified dihedral angles are varied, as shown in Figure 1b, resulting in polymer main chains with different planarity. The torsion angles between the DBP unit and the neighboring thiophene rings (φ_3 and φ_4) are very similar around 23° no matter what substituted groups are incorporated at the BT unit. In addition, it is reasonable for the larger angles (φ_1 and φ_2) around 13° between the thiophene and BT block for **PDBPTBT-2** due to the steric hindrance aroused from the ethylhexyloxy (OEH) groups substituted at the BT unit. When the OEH groups are replaced by the linear *n*-octyloxy chains in **PDBPTBT-3**, they are decreased to 6−7°, indicating better planarity of the polymer backbones. However, when the two *n*-octyloxy chains are reduced to one in **PDBPTBT-4**, it is surprising that both of the dihedral angles (φ_1 and φ_2) are as low as 1.4° and 0.5°, respectively, which is clearly elucidated by the side view of these **PDBPTBT** dimers in Figure 1b that the

DOI: 10.1021/acsami.6b11348
ACS Appl. Mater. Interfaces 2016, 8, 31348−31358

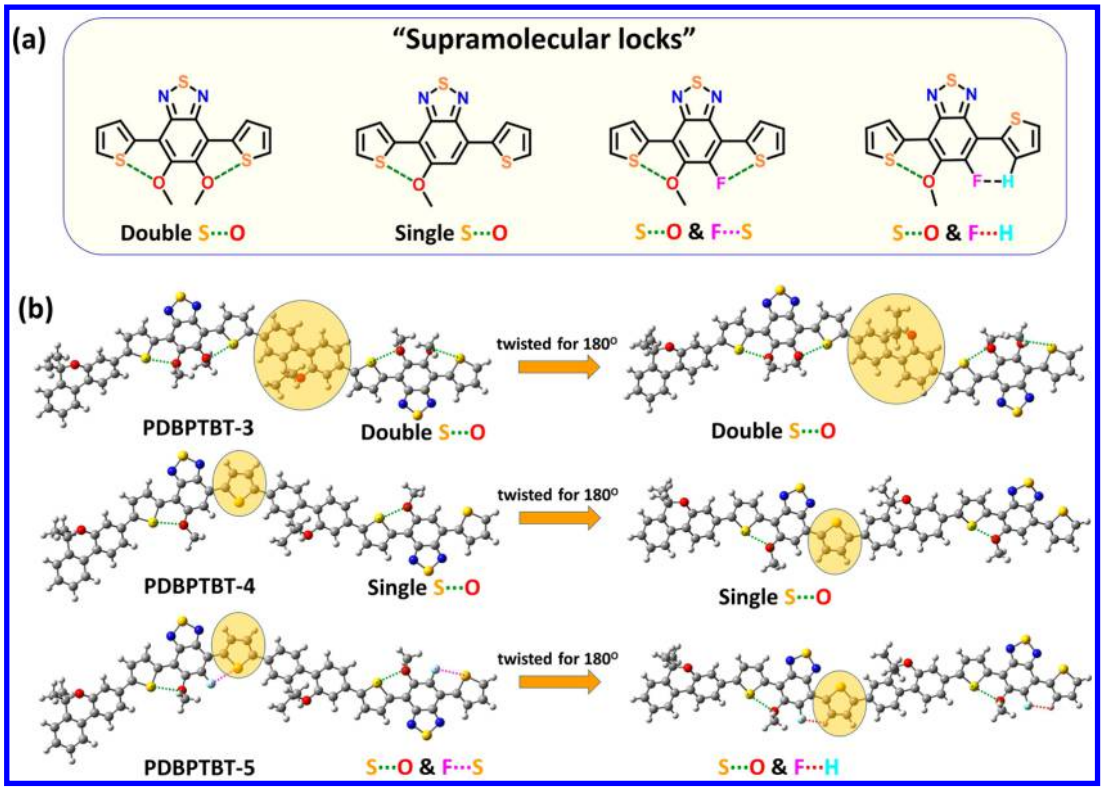

Figure 2. (a) Supramolecular locks at the BT fragments; (b) diagrams to demonstrate changes for the backbone curvatures of the polymers by twisting their linking units (DBP and/or thiophene).

alkyloxy group is in the same plane of the conjugated backbones for **PDBPTBT-4**, whereas the alkyloxy groups are out of plane in the other polymers. Finally, when the proton at the BT units of **PDBPTBT-4** is replaced by the electron-withdrawing fluorine atom in **PDBPTBT-5**, the alkyloxy group is pushed to the position out of plane again.

Each repeating unit of **PDBPTBT** includes four conjugated segments: one DBP unit, two thiophene units, and one BT unit with different substituted group. However, due to the asymmetrical properties of the DBP unit and some BT units, there are seven types of bonds, and the corresponding fragments are shown in Figure 1c. Relaxed potential energy scans (PES) for conformational preference of these segments have been studied, and the results indicate that the preferential configuration will not be influenced by the connection manners between the thiophene and DBP unit. However, in the five thiophene and BT segments in Figure 1c, the popular configurations are those with torsion angles around 0° (i.e., a *trans* formation).

In the meanwhile, intermolecular interactions of S···O, F···H, and F···S have been well-recognized in the similar conjugated polymer system and there are four possible kinds of "supramolecular conformation locks" in thiophene−BT fragments among these **PDBPTBT** polymers in Figure 2a. As in **PDBPTBT-2** and **PDBPTBT-3**, because of the double S···O interactions, the configuration of the thiophene−BT moieties could be locked-up in an energy preferred "*trans*, *trans*" conformation. But in **PDBPTBT-4**, there is only one "lock" at the thiophene−BT fragment, so the other thiophene unit could be freely rotated, and a "*trans*, *cis*"[24] conformation might be coexisted with the "*trans*, *trans*" structure according to the relaxed PES result. As the hydrogen atom is replaced by the fluorine in **PDBPTBT-5**, two pairs of the supramolecular locks are generated as shown in Figure 2a, which should be more likely to have two type conformations compared with **PDBPTBT-4**. As the rotation of the DBP units will not affect the conformations of the backbones in Figure 2b, the main concerns are focused on rotation of the thiophene ring because it might produce different conformations. Obviously, with the "*trans*, *cis*" configurations, the polymer backbones will become more rigid and straight, which may generate varied packing properties in XRD characterization and result in diverse photovoltaic properties.

Synthesis. The lactone compound **1** could be efficiently synthesized via the Baeyer−Villiger oxidation according to our previous reported method.[14] After attacking by octylmagnesium bromide and carrying out the dehydration reaction catalyzed under *p*-toluene sulfonic acid (PTSA), the 3,8-dibromo-6*H*-dibenzo[*b*,*d*]pyran (**3**) was obtained in a high yield of 91%. Finally, Miyaura reaction of **3** and bis(pinacolato)diboron with $Pd(dppf)_2Cl_2$ as the catalyst precursor afforded 2,2′-(6,6-dioctyl-6*H*-dibenzo[*c*]pyran-3,8-diyl)-bis(4,4,5,5-tetramethyl-1,3,2-dioxaborolane) (**M1**) in a yield of 56%.[14]

Generally, the types and density of the alkyl chains introduced onto the donor or acceptor unit will greatly influence the polymer processability, mainchain packing, and phase separation in the blend films. Our previous study indicated that the branched alkyloxy chains on BT (**M2**) can greatly improve the solubility of the final polymer, but the photovoltaic performance decreased in comparison to the one without the branched alkyloxy chains. Therefore, three different kinds of BT-based comonomers (**M3**, **M4**, and **M5**) were selected as the acceptor for the polymer design: mantaining the solubility on the one hand and making best use of supramolecular interactions to assist the intramolecular rigidification and mainchain packing on the other hand. In addition,

DOI: 10.1021/acsami.6b11348
ACS Appl. Mater. Interfaces 2016, 8, 31348−31358

Scheme 1. Synthesis of DBP Monomer (M1) and Polymers (PDBPTBT-2 to 5)

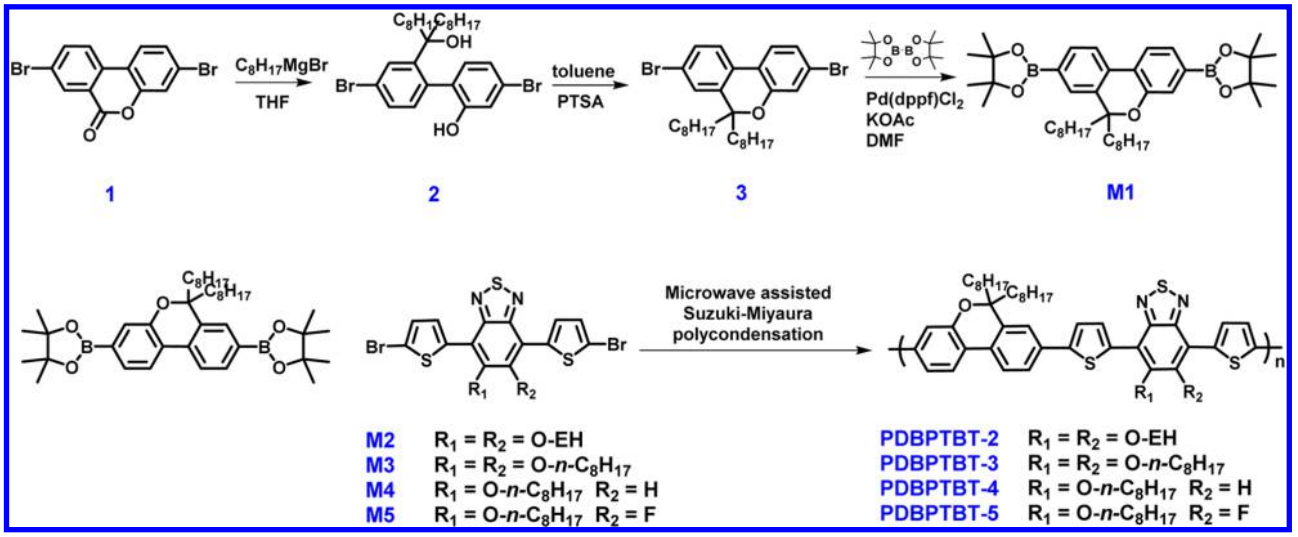

microwave-assisted Suzuki polycondensation were applied aiming at elevating the molecular weights of the final polymers (Scheme 1).

Molecular Weights and Thermal Properties. The introduction of flexible alkoxy chains on the benzothiadiazole ring guarantees good processability for the as-synthesized polymers. Polymer **PDBPTBT-2** and **PDBPTBT-3** can be fully dissolved in chloroform (CF), chlorobenzene (CB), 1,2-dichlorobenzene (DCB), and 1,2,4-trichlorobenzene (TCB) at elevated temperature. However, with the single alkoxy-chain-substituted **PDBPTBT-4** and **PDBPTBT-5**, they only can be partially dissolved in CF, but fully dissolved in CB, DCB and TCB at elevated temperature above 80 °C. The GPC results are summarized in Table 1 and the number-averaged molecular weight of **PDBPTBT-2** is greatly improved from 10.5 kg/mol by conventional heating[14] to 51.4 kg/mol via the application of the microwave-assisted polymerization. **PDBPTBT-5** reached an even higher M_w of 160.0 kg/mol, and the high molecular weights of the **PDBPTBT** polymers indicated they are potential donor candidates for high efficiency PSCs. Thermogravimetric analysis (TGA) studies, as shown in Figure 3, revealed that all the four polymers were stable above 315 °C, and **PDBPTBT-4** presented a higher 5% weight loss temperature among the polymers up to 369 °C due to a lower concentration of the alkyloxy chains.

Table 1. Molecular Weights and Thermal Properties of Polymers

polymer	M_n (kg/mol)	M_w (kg/mol)	PDI	T_d (°C)
PDBPTBT-2	51.4	99.3	1.93	315
PDBPTBT-3	21.1	41.9	1.99	324
PDBPTBT-4	62.9	85.3	1.36	369
PDBPTBT-5	33.4	160.0	4.79	331

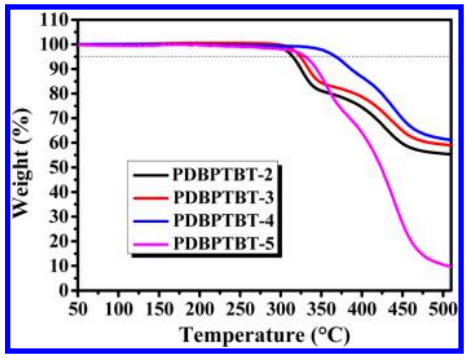

Figure 3. TGA analysis plots of these polymers at a heating rate of 10 °C/min under N_2.

Optical Properties. UV−vis absorption spectra of **PDBPTBT-2** to **PDBPTBT-5** in CB solutions and thin films are shown in Figure 4, and the details are listed in Table 2. All polymers present broad absorption ranging from 300 to 700 nm with two peaks located around 550 nm (Band I) and 400 nm (Band II), respectively. The linear-octyloxy-chain-substituted **PDBPTBT-3** presents a bathochromic-shifted absorption spectrum compared with the branched-alkyloxy-chain-substituted **PDBPTBT-2**. The mono-octyloxy-substituted **PDBPTBT-4** displays a most red-shifted absorption spectrum with an onset at 652 nm in Figure 4a due to the reduced φ_1 and φ_2 according to the DFT prediction (Figure 1 b). For the fluorine-substituted **PDBPTBT-5**, the introduction of fluorine atom induces a steric effect that can increase the φ_1, reduce the effective conjugation length, and produce a blue shift of the spectrum with an absorption onset at 636 nm. Meanwhile, clear shoulder peaks around the intramolecular charge transfer (ICT) band (Band I) were observed in solutions for **PDBPTBT-3**, **4**, and **5**, which might be originated from the strong $\pi-\pi$ interaction and the aggregation of the conjugated backbones. In addition, the appearance of the shoulder peaks in **PDBPTBT-3** demonstrated that linear octyloxy chains could result in better planarity of the backbones and stronger intermolecular interactions in comparison with **PDBPTBT-2**. Further enhancement was observed for **PDBPTBT-5**, which can be ascribed to the double supramolecular lock-up effects leading to rigidification of the polymer main chain and stronger $\pi-\pi$ stacking. As in thin films, all absorption curves became slightly broader, and the absorption band edge red-shifted a little bit. It is interesting that the spectral shape and maximum absorption wavelength of the **PDBPTBT** series polymers in films (in Figure 4b) were almost identical to that of their corresponding CB solutions at room temperature, despite a slight bathochromic shift. These results indicated that the polymer chains in solutions at room temperature already

DOI: 10.1021/acsami.6b11348
ACS Appl. Mater. Interfaces 2016, 8, 31348−31358

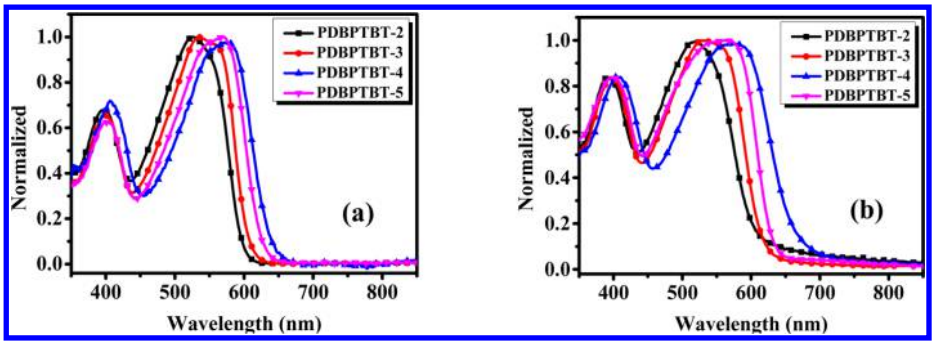

Figure 4. Normalized UV−vis absorption spectra of **PDBPTBT** series polymers (a) in dilute CB solutions and (b) as thin films on quartz substrates.

Table 2. Photophysical Properties and Molecular Energy Levels of the Polymers

	in solution		in film				
polymer	λ_{max} (nm)	λ_{onset} (nm)	λ_{max} (nm)	λ_{onset} (nm)	E_g^{opt} (eV)	HOMO (eV)	LUMO (eV)
PDBPTBT-2	512	610	520	614	2.02	−5.51	−3.49
PDBPTBT-3	532	619	532	625	1.98	−5.44	−3.46
PDBPTBT-4	579	652	579	683	1.82	−5.32	−3.50
PDBPTBT-5	551	636	562	638	1.94	−5.57	−3.63

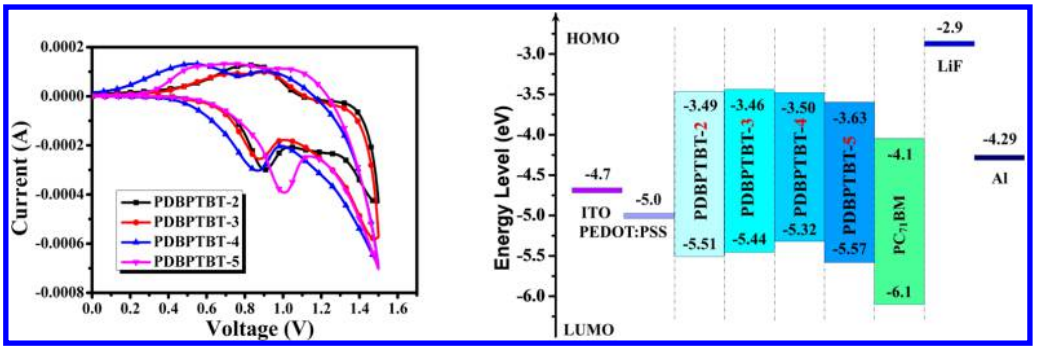

Figure 5. Cyclic voltammograms (left) of **PDBPTBT 2−5** films in 0.1 M Bu_4NPF_6−CH_3CN solutions at a scanning rate of 100 mV/s. Energy level diagrams (right) of **PDBPTBT 2−5** donor and $PC_{71}BM$ acceptor.

formed strong aggregation. It is recognized that such strong aggregation generally caused by the enhanced planarity of the polymer backbones may lead to higher charge carrier mobility and efficient photocurrent generation in photovoltaic devices.[26,27] The optical band gaps of **PDBPTBT-2** to **5** are 2.02, 1.98, 1.82, and 1.94 eV, respectively, and **PDBPTBT** series polymers are therefore classified as wide band gap polymers.

Energy Levels. DFT quantum chemistry calculation at the B3LYP/6-31G (d,p) level is also employed to predict the highest occupied molecular orbital (HOMO) and the lowest unoccupied molecular orbital (LUMO) levels of the four polymers. The optimized geometries and the electron distributions of the HOMO and LUMO levels of these polymers are very similar, as shown in Figure S1, yet the DFT results could provide some tendency of the HOMO energy levels as following: $HOMO_{PDBPTBT-5} < HOMO_{PDBPTBT-2} = HOMO_{PDBPTBT-3} < HOMO_{PDBPTBT-4}$. Because the HOMO and LUMO energy levels are crucial to the photovoltaic performance of PSCs, the electrochemical properties of **PDBPTBT** polymers were investigated by cyclic voltammetry with a standard three-electrode electrochemical cell in acetonitrile solution containing 0.1 M Bu_4NPF_6 at room temperature under a nitrogen atmosphere with a scanning rate of 100 mV/s. Ag/$AgNO_3$ was used as the reference electrode, and a standard ferrocene/ferrocenium redox system was used as the internal standard. The CV curves of **PDBPTBT-2** to **5** are shown in Figure 5, and their HOMO energy levels are −5.51, −5.44, −5.32, and −5.57 eV, respectively, which were calculated from the onset oxidation potential (E_{ox}) of these polymers according to the following equations: $E_{HOMO} = -[(E_{ox} - E_{(Fc/Fc+)} + 4.8]$ (eV). The LUMO energy levels of these **PDBPTBT** polymers were calculated to be in the range of −3.46 to −3.63 eV according to $E_{LUMO} = E_{HOMO} + E_g$, which are higher than that of $PC_{71}BM$ (−4.1 eV), guaranteeing the efficient photoinduced electron transfer from the polymer donor to $PC_{71}BM$ acceptor. From the energy level diagrams in Figure 5, it is obvious that the type and quantity of the alkyl side chains have great influences on the HOMO and LUMO energy levels, even the conjugated backbones of **PDBPTBT-2** to **4** are very similar. It appears that linear and fewer alkyloxy chains could elevate the HOMO energy levels but have a tiny influence on the LUMO energy levels. However, when the fluorine is introduced into the copolymer system, the HOMO and LUMO energy levels descend together and the lowest HOMO of −5.57 eV was obtained for **PDBPTBT-5**. Considering that the open circuit voltage (V_{oc}) of PSCs is correlated to the difference in the LUMO energy level of the acceptor and the HOMO energy level of the polymer donor, the deep HOMO level of these **PDBPTBT** series polymers should give higher V_{oc} PSCs.

DOI: 10.1021/acsami.6b11348
ACS Appl. Mater. Interfaces 2016, 8, 31348−31358

X-ray Diffraction Analysis. As shown in Figure 6, all **PDBPTBT** polymers exhibit two diffraction peaks in the XRD

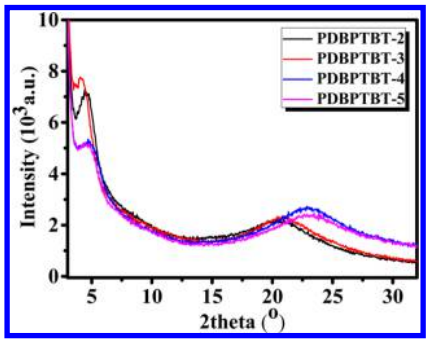

Figure 6. XRD patterns of spin-coated **PDBPTBT** films.

curves. The first peaks around small-angle region, which reflex the distance of polymer backbones separated by the flexible side chains, are located at 2θ of 4.46°, 4.16°, 4.77°, and 4.77° for **PDBPTBT-2** to **PDBPTBT-5**, corresponding to the distances of 19.79, 21.22, 18.50, and 18.50 Å, respectively. The second peaks around the wide-angle region, which reflex the $\pi-\pi$ stacking distances between polymer backbones, are located at 2θ of 20.47° for **PDBPTBT-2**, 20.91° for **PDBPTBT-3**, 22.86° for **PDBPTBT-4**, and 22.96° for **PDBPTBT-5**, corresponding to distances of 4.33, 4.24, 3.89, and 3.87 Å, respectively. The results of **PDBPTBT-2** and **PDBPTBT-3** demonstrated that the branched side chains will hamper the close and ordered packing of polymer chains in the solid state compared with the linear side chains, and the $\pi-\pi$ stacking distance between polymer backbones can be slightly tuned by the side chains. In addition, tuning the density of alkyl side chains is another effective way to increase the ordered $\pi-\pi$ stacking of polymer chains in the solid thin films. The decreased d-spacing and $\pi-\pi$ stacking distances for **PDBPTBT-4** and **PDBPTBT-5** might be the evidence to the coexistence of straight and rigid polymer chains in the solid state, as discussed in Figure 2b.

SCLC Mobilities. Hole (μ_h) and electron (μ_e) mobilities are important factors to the charge transport in PSCs. Higher mobility values are desired for high-performance devices. Therefore, the μ_h and μ_e of the **PDBPTBT**:$PC_{71}BM$ blend were investigated via the space charge limited current (SCLC) method in typical device structures of ITO/PEDOT:PSS/polymer:$PC_{71}BM$/Au and ITO/ZnO/polymer:$PC_{71}BM$/LiF/Al, respectively. The averaged μ_h of **PDBPTBT-2**:$PC_{71}BM$, **PDBPTBT-3**:$PC_{71}BM$, **PDBPTBT-4**:$PC_{71}BM$, and **PDBPTBT-5**:$PC_{71}BM$ were evaluated to be 2.32×10^{-5}, 2.77×10^{-5}, 3.31×10^{-5}, 5.16×10^{-5} $cm^2\ V^{-1}\ s^{-1}$, respectively, and the corresponding μ_e are 3.30×10^{-6}, 4.21×10^{-6}, 6.15×10^{-6}, 1.42×10^{-5} $cm^2\ V^{-1}\ s^{-1}$, respectively (shown in Table 3 and Figure S3–S4). Although these four polymers had very similar conjugated backbones, they presented different charge carrier transport properties, which may be attributed to the different packing style in the solid state caused by the varied substituents on the BT moieties.

Photovoltaic Properties. Photovoltaic properties of the **PDBPTBT** polymers were first investigated in a typical device architecture of ITO/PEDOT:PSS/active layer/LiF/Al in this work. The performance of devices was optimized by varying the weight ratio of polymer to $PC_{71}BM$, concentration of blend solution, additive effects, and interfacial layers. For polymers **PDBPTBT-2**, **3**, and **4**, the optimum ratio of polymer to $PC_{71}BM$ was 1:3 (w/w), and their PCEs reached 2.02%, 3.23%, and 3.87%, respectively. However, 1:1.5 appears to be the best ratio of polymer to $PC_{71}BM$ for **PDBPTBT-5**, and the preliminary results as shown in Table S1 indicated that **PDBPTBT-5** with a PCE of 5.32% (V_{oc} = 0.90 V, J_{sc} = 10.60 mA/cm^2, and FF = 0.56) could be a good candidate as polymer donor. The better photovoltaic performance of **PDBPTBT-5** may be attributed to the rigid and straight conformation of polymer main chains induced by the double supramolecular conformation locks. Subsequently, different additives such as 1,8-diiodooctane (DIO), chloronaphthalene (CN) and diphenylether (DPE) were utilized to optimize the device performance of **PDBPTBT-5**, and the results are listed in Table S2. Generally, DIO and DPE provided better PCEs than CN, but DIO still seems to be the universal and the best choice for **PDBPTBT** series polymers after integral analysis of the photovoltaic results. After careful optimization of the DIO concentration from 1% to 5% (volume ratio), a PCE of 5.66% (V_{oc} = 0.91 V, J_{sc} = 10.80 mA/cm^2, and FF = 0.58) was achieved under the optimum DIO percentage of 2%. When the other three polymers (**PDBPTBT-2**, **3**, and **4**) were applied with DIO at this concentration, their PCEs were improved to 3.28%, 3.99%, and 4.10%, respectively. The final optimized results are summarized in Table 3. As shown in Figure 7, external quantum efficiencies (EQE) were measured and all polymers exhibited broad photo to current responses in the range of 300 to 700 nm. These four polymers exhibited similar EQE curves in shape from **PDBPTBT-2** to **PDBPTBT-5** but varied in intensity. In addition, **PDBPTBT-5** displayed a high intensity close to 70%.

Meanwhile, a key issue to achieve better photovoltaic performance is to select the appropriate interlayer between active layer and the electrode.[28−30] PFN-based water-/alcohol-soluble conjugated polymers have been proven to be a good

Table 3. Photovoltaic Performances and SCLC Mobilities of Polymer:$PC_{71}BM$ Blend Films

polymer	additive (v%)	V_{oc} (V)	J_{sc} (mA/cm^2)	FF	PCE (%)	μ_h ($cm^2\ V^{-1}\ s^{-1}$)	μ_e ($cm^2\ V^{-1}\ s^{-1}$)
PDBPTBT-2:$PC_{71}BM$ = 1:3	w/o	0.96	5.51	0.38	2.02	---	---
PDBPTBT-2:$PC_{71}BM$ = 1:3	2% DIO	0.90	6.10	0.59	3.28	2.32×10^{-5}	3.30×10^{-6}
PDBPTBT-3:$PC_{71}BM$ = 1:3	w/o	0.86	6.98	0.54	3.23	---	---
PDBPTBT-3:$PC_{71}BM$ = 1:3	2% DIO	0.80	8.03	0.62	3.99	2.77×10^{-5}	4.21×10^{-6}
PDBPTBT-4:$PC_{71}BM$ = 1:3	w/o	0.79	8.40	0.58	3.87	---	---
PDBPTBT-4:$PC_{71}BM$ = 1:3	2% DIO	0.75	9.42	0.58	4.10	3.31×10^{-5}	6.15×10^{-6}
PDBPTBT-5:$PC_{71}BM$ = 1:1.5	w/o	0.90	10.60	0.56	5.32	---	---
PDBPTBT-5:$PC_{71}BM$ = 1:1.5	2% DIO	0.91	10.80	0.58	5.66	5.16×10^{-5}	1.42×10^{-5}
PDBPTBT-5:$PC_{71}BM$ = 1:1.5	2% CN	0.92	9.67	0.55	4.95	---	---
PDBPTBT-5:$PC_{71}BM$ = 1:1.5	2% DPE	0.91	10.50	0.58	5.50	---	---

DOI: 10.1021/acsami.6b11348
ACS Appl. Mater. Interfaces 2016, 8, 31348−31358

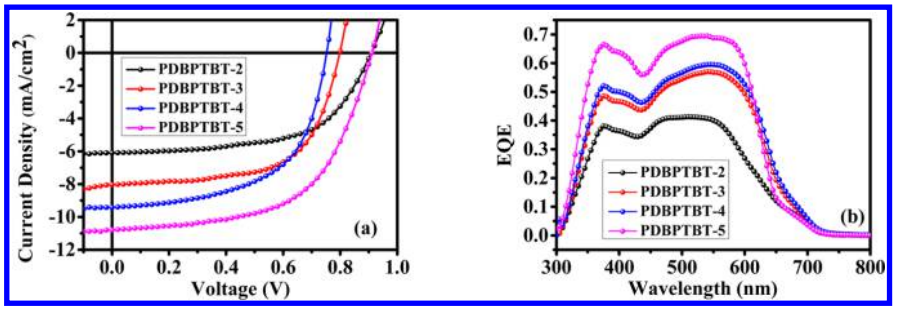

Figure 7. (a) $J-V$ curves of PSCs fabricated from the blend of **PDBPTBT**:$PC_{71}BM$ in DCB; (b) EQE curves of the optimum PSCs based on different **PDBPTBT** donor materials with 2% DIO as the additive.

Table 4. Interlayer Impact on the Photovoltaic Performances of PDBPTBT-5:$PC_{71}BM$ = 1:1.5 Blend Films

polymer	additive (v%)	interlayer	V_{oc} (V)	J_{sc} (mA/cm^2)	FF	PCE (%)
PDBPTBT-5:$PC_{71}BM$ = 1:1.5	2% DIO	MeOH	0.94	10.80	0.60	6.08
PDBPTBT-5:$PC_{71}BM$ = 1:1.5	2% DIO	PFN	0.95	10.71	0.66	6.72
PDBPTBT-5:$PC_{71}BM$ = 1:1.5	2% DIO	PFN-OX	0.96	11.09	0.67	7.06

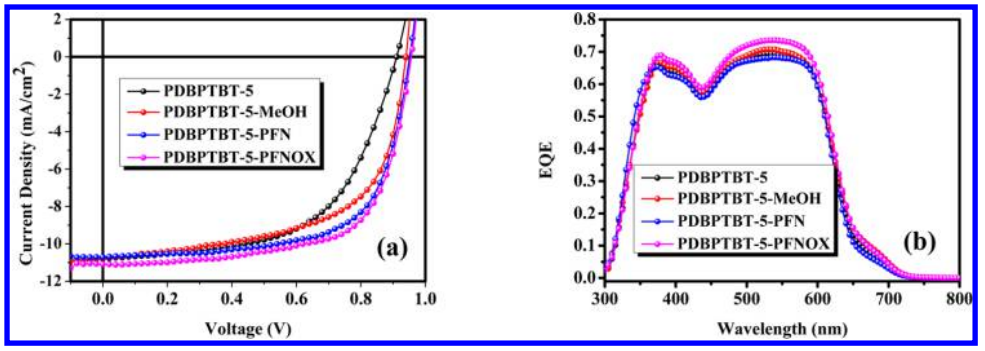

Figure 8. (a) $J-V$ curves and (b) EQE curves of PSCs fabricated from the blend of **PDBPTBT-5**:$PC_{71}BM$ in DCB with 2% DIO as the additive with different interfacial layers.

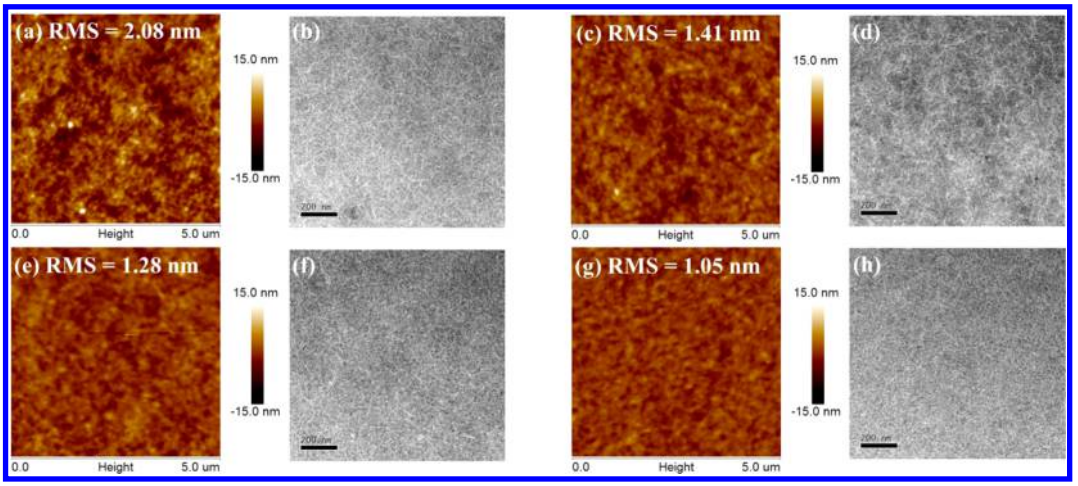

Figure 9. AFM and TEM images of polymer and $PC_{71}BM$ blend film at the optimized ratios with 2% DIO. (a) and (b), **PDBPTBT-2:**$PC_{71}BM$ (1:3); (c) and (d), **PDBPTBT-3:**$PC_{71}BM$ (1:3); (e) and (f), **PDBPTBT-4:**$PC_{71}BM$ (1:3); (g) and (h), **PDBPTBT-5:**$PC_{71}BM$ (1:1.5).

electron extraction layer,[31−34] so in this work, PFN and PFN-OX are employed for the further optimization of the photovoltaic devices. For a comparison, the control device is fabricated by spin-coating methanol on top of the active layer, which is also utilized as a post-treatment for the device fabrication due to its impact on the phase separation. The final results indicated that the PCEs were all elevated after washing the active layer with methanol and introducing an interlayer of PFN. The control device gave a PCE of 6.08%, and it was increased to 6.72% after the introduction of the PFN layer. The best PCE of 7.06% (V_{oc} = 0.96 V, J_{sc} = 11.09 mA/cm^2, and FF = 0.66) was finally achieved by the PFN-OX modified device. The detailed device optimization results are provided in Table 4. The $J-V$ and EQE curves are shown in Figure 8.

Morphological Properties. Morphology of the blend films can largely affect the charge separation and transport. In order

DOI: 10.1021/acsami.6b11348
ACS Appl. Mater. Interfaces 2016, 8, 31348−31358

to get further insight into the relationship between polymer structures and the device performances, morphologies of blend films were investigated by atomic force microscopy (AFM) in a tapping-mode. Generally, the ideal morphology of the active layer is a bicontinuous interpenetrating network, and the optimum phase-separated domain size should be around 10−20 nm to facilitate efficient exciton dissociation and charge transport. As shown in Figure 9a, the **PDBPTBT-2:**$PC_{71}BM$ blend film displays an apparent phase separation with a root mean square (rms) roughness of 2.08 nm, and it is reduced to 1.41 nm for the **PDBPTBT-3:**$PC_{71}BM$ blend film in Figure 9c, when the branched side chains are replaced by the linear octyloxy chains. Both of the two blend films present a large domain size above 100 nm, which markedly exceeds the exciton diffusion length and greatly reduces the efficiency of exciton dissociation, leading to lower J_{sc} and FF values. In contrast, **PDBPTBT-4:**$PC_{71}BM$ blend film shows similar rms (1.28 nm) to that of **PDBPTBT-3** when the density of alkyloxy side chains is reduced to one at each BT moiety, but the blend film becomes more homogeneous, implying good miscibility between **PDBPTBT-4** and $PC_{71}BM$ (Figure 9e). The introduction of the fluorine atoms in **PDBPTBT-5** does not seem to have an influence on the phase-separated domain size and miscibility with $PC_{71}BM$ in the blend film compared with that of **PDBPTBT-4**, but the rms is further reduced to 1.05 nm as shown in Figure 9g.

Because AFM images can only provide the surface morphology information for the blend films, transmission electron microscopy (TEM) was further empolyed to investigate the composition and in-depth structures of the active layers. Nanostructures with curved fibrils and straight nanofibers are distinct in the blend films of **PDBPTBT-2:**$PC_{71}BM$ and **PDBPTBT-3:**$PC_{71}BM$, respectively, but the larger diameters of the nanostructures and the poor miscibility with $PC_{71}BM$ are obviously preferable neither for efficient exciton dissociation nor for balanced charge transport. As for the blend films of **PDBPTBT-4:**$PC_{71}BM$ and **PDBPTBT-5:**$PC_{71}BM$ shown in Figure 9f,h, finer phase separation is observed for both polymers at nanoscale and the bicontinuous interpenetrating network is especially uniform for **PDBPTBT-5**. On the basis of the AFM and TEM results, we can conclude that the density and type of the side chains in **PDBPTBT** polymers have imparted a great influence on the morphology of blend films in nanoscale as well as the photovoltaic performance.

CONCLUSIONS

Four DBP-based conjugated copolymers (**PDBPTBT-2**, **PDBPTBT-3**, **PDBPTBT-4**, and **PDBPTBT-5**) carrying different alkyl side chain placement or fluorine substitution were synthesized via microwave assisted Suzuki polymerization. Although they have similar conjugated backbones, the diverse "supramolecular conformation locks" existing in the polymer systems could result in varied conformations and curvatures. According to the theoretical calculation results, we could predict that the backbones of **PDBPTBT** polymers generally possess zigzag conformation, but straight and rigid configuration of **PDBPTBT-5** is likely to coexist in the meanwhile due to the supramolecular conformation locks of "S···O and F···H/F···S". XRD measurements revealed that **PDBPTBT-4** and **PDBPTBT-5** can form closer interchain packing and $\pi-\pi$ stacking than the other two polymers, agreeing with the quantum chemistry calculation results. In addition, it has been clearly demonstrated that the photophysical properties and energy levels of these **PDBPTBT** polymers could be tuned by the type and density of the alkyloxy chains as well as the fluorine substitution. All polymers were optimized in the OPV device fabrication and the best PCE of 5.32% was obtained for **PDBPTBT-5**. In addition, the varied PCEs of these **PDBPTBT** polymers are also related to morphology differences aroused by the type and density of the side chains. Finally, with 2% DIO as the additive and PFN-OX as the buffer layer, the devices achieved a PCE of 7.06% (V_{oc} = 0.96 V, J_{sc} = 11.09 mA/cm^2, and FF = 0.67), indicating **PDBPTBT-5** is a promising wide band gap donor material for PSCs.

EXPERIMENTAL SECTION

Materials and Methods. All commercial chemicals were used without further purification. **M1** to **M5** were synthesized according to our previous report.[14,19,20] Tetrahydrofuran and toluene were freshly distilled from sodium containing benzophenone prior to use. The microwave-assisted polymerization was carried out in the Discover (CEM Corp.) microwave reactor. UV−visible absorption spectra were characterized by a UV-1601pc spectrophotometer. Molecular weights (number-average (M_n) and weight-average (M_w)) of the final polymers were tested using Agilent Technologies 1200 series GPC at 80 °C with chlorobenzene as the eluent and narrow polydispersity polystyrene as the standard. Atomic force microscopy (AFM) images of the active layers were taken on a Nanoscope IIIa Dimension 3100 under a tapping mode. Thermogravimetric analysis (TGA) was performed on a PerkinElmer Pyris 1 analyzer under a nitrogen atmosphere with a heating rate of 10 °C/min. CHI 600E Electrochemical Analyzer was employed for the electrochemical measurements. Silica gel with 300−400 mesh was utilized for the column chromatography. ^{1}H NMR spectra were taken on a 400 MHz spectrometer using chloroform-*d* ($CDCl_3$) as solvent.

General Procedures for Polymerization. To a microwave tube was charged with a equivalent of BDP monomer (**M1**) and **BT**-based monomers (**M2**, **M3**, **M4** or **M5**), $Pd(PPh_3)_4$ (3 mg). After purging with argon for 20 min, H_2O (1.5 mL), toluene (9 mL), THF (3 mL), $NaHCO_3$ (200 mg), and one drop of trioctylmethylammonium chloride were added under the protection of argon, and it was carefully degassed before and after $Pd(PPh_3)_4$ (5 mg) was added. The reaction mixture was refluxed for 2 h in a microwave reactor under argon atmosphere. After it was cooled to room temperature, phenylboronic acid (10 mg) was added, and the reaction was refluxed for 30 min; then 1-bromobenzene (0.05 mL) was added, and the reaction was refluxed for another 30 min. When the reaction mixture was then allowed to cool to room temperature, it was extracted with chloroform. The organic phase was collected and washed with water (50 mL × 3). After most of the solvent was removed by rotary evaporation, the residue was poured into acetone (80 mL), and the precipitate was filtered through a Soxhlet thimble and subjected to Soxhlet extraction sequentially with different solvents (acetone, hexane, dichloromethane, and chloroform). For polymer **PDBPTBT-2** and **PDBPTBT-3**, only chloroform portion was collected, condensed, and precipitated in acetone (80 mL) to afford the final products. As for polymer **PDBPTBT-4** and **PDBPTBT-5**, the residue was refluxed and dissolved in hot chlorobenzene; after filtration, the resulted condensed solution was also precipitated into acetone (80 mL) to afford the final products.

Synthesis of ***PDBPTBT-2****.* According to the general polymerization method, monomer **M1** (119.0 mg, 0.1670 mmol, 1.0 equiv) and monomer **M2** (110.0 mg, 0.1670 mmol, 1.0 equiv) were used. **PBDPTBT-2** was obtained as a dark red solid (126 mg, 68%). M_n and PDI measured by high-temperature GPC calibrated with polystyrene standards are 51.4 kg/mol and 1.93, respectively. ^{1}H NMR (400 MHz, $CDCl_3$,): δ 8.37−8.23 (mbr, 2H), 7.88−7.76 (mbr, 3H), 7.56−7.30 (mbr, 5H), 4.03 (br, 4H), 2.01 (br, 4H), 1.73−1.16 (mbr, 42H), 1.04−0.73 (mbr, 18H).

DOI: 10.1021/acsami.6b11348
ACS Appl. Mater. Interfaces 2016, 8, 31348−31358

*Synthesis of **PDBPTBT-3**.* According to the general polymerization method, monomer **M1** (119.0 mg, 0.1670 mmol, 1.0 equiv) and monomer **M3** (110.0 mg, 0.1670 mmol, 1.0 equiv) were used. **PBDPTBT-3** was obtained as a dark red solid (180 mg, 96%). M_n and PDI measured by GPC calibrated with polystyrene standards are 21.1 kg/mol and 1.99, respectively. ^{1}H NMR (400 MHz, $CDCl_3$,): δ 8.63−8.46 (mbr, 2H), 7.90−7.67 (mbr, 3H), 7.56−7.31 (mbr, 5H), 4.32−4.10 (mbr, 4H), 2.17−1.83 (mbr, 8H), 1.77−1.11 (mbr, 44H), 0.94−0.75 (mbr, 12H).

*Synthesis of **PDBPTBT-4**.* According to the general polymerization method, monomer **M1** (123.5 mg, 0.1870 mmol, 1.0 equiv) and monomer **M4** (110.0 mg, 0.1870 mmol, 1.0 equiv) were used. **PBDPTBT-4** was obtained as a dark red solid (63.8 mg, 34%). M_n and PDI measured by GPC calibrated with polystyrene standards are 62.9 kg/mol and 1.36, respectively. ^{1}H NMR (400 MHz, $CDCl_3$,): δ 8.71−8.51 (mbr, 2H), 8.25 (br, H), 7.87−7.57 (mbr, 3H), 7.55−7.35 (mbr, 6H), 4.56−4.32 (mbr, 2H), 2.18−2.03 (mbr, 4H), 1.44−1.15 (mbr, 36H), 0.99−0.7 (mbr, 9H).

*Synthesis of **PDBPTBT-5**.* According to the general polymerization method, monomer **M1** (123.3 mg, 0.1873 mmol, 1.0 equiv) and monomer **M5** (113.2 mg, 0.1873 mmol, 1.0 equiv) were used. **PBDPTBT-5** was obtained as a dark red solid (94.25 mg, 59%). M_n and PDI measured by GPC calibrated with polystyrene standards are 33.4 kg/mol and 4.79, respectively. ^{1}H NMR (400 MHz, $CDCl_3$,): δ 8.65−8.50 (mbr, 1H), 8.30 (br, 1H), 7.85−7.60 (mbr, 3H), 7.57−7.30 (mbr, 5H), 4.32−4.18 (mbr, 2H), 2.50−2.12 (mbr, 4H), 1.39−1.14 (mbr, 36H), 0.92−0.77 (mbr, 9H).

OPV Device Fabrication and Characterization. OPV devices were made with a general configuration of ITO/PEDOT:PSS/active layer/LiF/Al. ITO with conductivity of 20 Ω/sq and PEDOT:PSS (Baytron P VP.AI 4083) were employed. A thin layer of PEDOT:PSS was prepared on top of the cleaned ITO substrate via spin-coating at 3500 rpm/s and subsequently dried at 120 °C for 20 min on a hot plate. The **PDBPTBT** polymer and $PC_{71}BM$ were blended at 90 °C in DCB before spin-coating, and the active layer was spin-coated at 1600 rpm for 60 s on top of PEDOT:PSS layer. The optimum concentrations for polymer **PDBPTBT-2** to **4** in DCB are the same at 6.3 mg/mL, and for **PDBPTBT-5**, the optimized concentration is 7.0 mg/mL. In addition, different additives such as DIO, CN, and DPE were utilized in the active layer for the device optimization. Then, a solution containing PFN or PFN-OX at a concentration of 0.2 mg/mL in methanol:acetic acid (100:1 v/v) was spin-coated onto the active layer to achieve ∼5 nm interlayer during the optimization. Finally, the top aluminum electrode was thermally evaporated with a thickness of 100 nm at a pressure of 10^{-4} Pa. Six cells were fabricated on one substrate, and the effective area in each cell is 4 mm^2. The solar cell device characterization was carried out on a computer controlled Keithley 2400 digital source meter with an AM1.5G AAA class solar simulator (model XES-70S1, SAN-EI, 100 mW cm^{-2}) as the white light source in a glovebox without encapsulation. The intensity was calibrated with a standard single-crystal Si photovoltaic cell.

Electrochemistry. The electrochemical properties of **PDBPTBT** polymers were investigated by cyclic voltammetry (CV) using 0.1 M tetrabutylammoniumhexafluorophosphate (Bu_4NPF_6) acetonitrile solution as the supporting electrolyte under an atmosphere of nitrogen. The characterization was carried out using a three-electrode arrangement in a single compartment cell. A Pt wire, an $Ag/AgNO_3$ electrode, and a slide of ITO glass coated with polymer film were used as the counter electrode, reference electrode and the working electrode, respectively.

■ ASSOCIATED CONTENT

Supporting Information

The Supporting Information is available free of charge on the ACS Publications website at DOI: 10.1021/acsami.6b11348.

Theoretical calculations results of **PDBPTBT** polymers; PSC device optimization results and SCLC mobilities of **PDBPTBT**:$PC_{71}BM$ blend (PDF)

■ AUTHOR INFORMATION

Corresponding Authors

*Email: songjs@henu.edu.cn.
*Email: zsbo@bnu.edu.cn.
*Email: hwang@henu.edu.

Notes

The authors declare no competing financial interest.

■ ACKNOWLEDGMENTS

This research was supported by NSFC (U1204212, 21404031, and 21272055), Program from Henan University (yqpy20140058), Innovation Scientists and Technicians Troop Construction Projects of Henan Province (C20150011).

■ REFERENCES

(1) You, J.; Dou, L.; Yoshimura, K.; Kato, T.; Ohya, K.; Moriarty, T.; Emery, K.; Chen, C. C.; Gao, J.; Li, G.; Yang, Y. A Polymer Tandem Solar Cell with 10.6% Power Conversion Efficiency. *Nat. Commun.* **2013**, *4*, 1446.

(2) Gong, X.; Li, C.; Lu, Z.; Li, G.; Mei, Q.; Fang, T.; Bo, Z. Anthracene-Containing Wide-Band-Gap Conjugated Polymers for High-Open-Circuit-Voltage Polymer Solar Cells. *Macromol. Rapid Commun.* **2013**, *34*, 1163−1168.

(3) Ding, D.; Wang, J.; Chen, W.; Qiu, M.; Ren, J.; Zheng, H.; Liu, D.; Sun, M.; Yang, R. Novel Wide Band Gap Polymers Based on Dithienobenzoxadiazole for Polymer Solar Cells with High Open Circuit Voltages over 1 V. *RSC Adv.* **2016**, *6*, 51419−51425.

(4) Zhao, K.; Wang, Q.; Xu, B.; Zhao, W.; Liu, X.; Yang, B.; Sun, M.; Hou, J. Efficient Fullerene-Based and Fullerene-Free Polymer Solar Cells Using Two Wide Band Gap Thiophene-Thiazolothiazole-Based Photovoltaic Materials. *J. Mater. Chem. A* **2016**, *4*, 9511−9518.

(5) Franco, S.; Garin, J.; de Baroja, N. M.; Perez-Tejada, R.; Orduna, J.; Yu, Y.; Lira-Cantu, M. New D-π-A-Conjugated Organic Sensitizers Based on 4*H*-Pyran-4-ylidene Donors for Highly Efficient Dye-Sensitized Solar Cells. *Org. Lett.* **2012**, *14*, 752−755.

(6) Cheng, Y.; Zhu, B.; Deng, Y.; Zhang, Z. In Vivo Detection of Cerebral Amyloid Fibrils with Smart Dicynomethylene-4*H*-Pyran-Based Fluorescence Probe. *Anal. Chem.* **2015**, *87*, 4781−4787.

(7) Andreu, R.; Galan, E.; Garin, J.; Herrero, V.; Lacarra, E.; Orduna, J.; Alicante, R.; Villacampa, B. Linear and V-Shaped Nonlinear Optical Chromophores with Multiple 4*H*-Pyran-4-ylidene Moieties. *J. Org. Chem.* **2010**, *75*, 1684−1692.

(8) Leung, M. K.; Chang, C. C.; Wu, M. H.; Chuang, K. H.; Lee, J. H.; Shieh, S. J.; Lin, S. C.; Chiu, C. F. 6-*N*,*N*-Diphenylaminobenzofuran-Derived Pyran Containing Fluorescent Dyes: A New Class of High-Brightness Red-Light-Emitting Dopants for Oled. *Org. Lett.* **2006**, *8*, 2623−2626.

(9) Shiraishi, Y.; Nakamura, M.; Hayashi, N.; Hirai, T. Coumarin-Spiropyran Dyad with a Hydrogenated Pyran Moiety for Rapid, Selective, and Sensitive Fluorometric Detection of Cyanide Anion. *Anal. Chem.* **2016**, *88*, 6805−6811.

(10) Lin, Q.; Bao, C.; Cheng, S.; Yang, Y.; Ji, W.; Zhu, L. Target-Activated Coumarin Phototriggers Specifically Switch on Fluorescence and Photocleavage Upon Bonding to Thiol-Bearing Protein. *J. Am. Chem. Soc.* **2012**, *134*, 5052−5055.

(11) Zhang, H.; Wang, C.; Jiang, T.; Guo, H.; Wang, G.; Cai, X.; Yang, L.; Zhang, Y.; Yu, H.; Wang, H.; Jiang, K. Microtubule-Targetable Fluorescent Probe: Site-Specific Detection and Super-Resolution Imaging of Ultratrace Tubulin in Microtubules of Living Cancer Cells. *Anal. Chem.* **2015**, *87*, 5216−5222.

(12) Dou, L.; Chen, C.-C.; Yoshimura, K.; Ohya, K.; Chang, W.-H.; Gao, J.; Liu, Y.; Richard, E.; Yang, Y. Synthesis of 5*H*-Dithieno[3,2-*b*:2ithie*d*]Pyran as an Electron-Rich Building Block for Donor−Acceptor Type Low-Bandgap Polymers. *Macromolecules* **2013**, *46*, 3384−3390.

(13) Lee, J. W.; Bae, S.; Jo, W. H. Synthesis of 6*H*-Benzo[*c*]-Chromene as a New Electron-Rich Building Block of Conjugated

DOI: 10.1021/acsami.6b11348
ACS Appl. Mater. Interfaces 2016, 8, 31348−31358

Alternating Copolymers and Its Application to Polymer Solar Cells. *J. Mater. Chem. A* **2014**, *2*, 14146−14153.
(14) Song, J. S.; Guo, Y. J.; Liu, L. J.; Wang, H. Efficient Synthesis of Dibenzopyran Building Block and Its Application in Organic Photovoltaics. *Dyes Pigm.* **2015**, *122*, 184−191.
(15) Li, G.; Zhao, B.; Kang, C.; Lu, Z.; Li, C.; Dong, H.; Hu, W.; Wu, H.; Bo, Z. Side Chain Influence on the Morphology and Photovoltaic Performance of 5-Fluoro-6-Alkyloxybenzothiadiazole and Benzodithiophene Based Conjugated Polymers. *ACS Appl. Mater. Interfaces* **2015**, *7*, 10710−10717.
(16) Zhang, S.; Yang, B.; Liu, D.; Zhang, H.; Zhao, W.; Wang, Q.; He, C.; Hou, J. Correlations among Chemical Structure, Backbone Conformation, and Morphology in Two Highly Efficient Photovoltaic Polymer Materials. *Macromolecules* **2016**, *49*, 120−126.
(17) Du, C.; Li, C.; Li, W.; Chen, X.; Bo, Z.; Veit, C.; Ma, Z.; Wuerfel, U.; Zhu, H.; Hu, W.; Zhang, F. 9-Alkylidene-9*H*-Fluorene-Containing Polymer for High-Efficiency Polymer Solar Cells. *Macromolecules* **2011**, *44*, 7617−7624.
(18) Jin, E.; Du, C.; Wang, M.; Li, W.; Li, C.; Wei, H.; Bo, Z. Dibenzothiophene-Based Planar Conjugated Polymers for High Efficiency Polymer Solar Cells. *Macromolecules* **2012**, *45*, 7843−7854.
(19) Li, G.; Kang, C.; Gong, X.; Zhang, J.; Li, C.; Chen, Y.; Dong, H.; Hu, W.; Li, F.; Bo, Z. 5-Alkyloxy-6-Fluorobenzo[*c*][1,2,5]Thiadiazole- and Silafluorene-Based D−A Alternating Conjugated Polymers: Synthesis and Application in Polymer Photovoltaic Cells. *Macromolecules* **2014**, *47*, 4645−4652.
(20) Qin, R.; Li, W.; Li, C.; Du, C.; Veit, C.; Schleiermacher, H. F.; Andersson, M.; Bo, Z.; Liu, Z.; Inganas, O.; Wuerfel, U.; Zhang, F. A Planar Copolymer for High Efficiency Polymer Solar Cells. *J. Am. Chem. Soc.* **2009**, *131*, 14612−14613.
(21) Huang, H.; Zhou, N.; Ortiz, R. P.; Chen, Z.; Loser, S.; Zhang, S.; Guo, X.; Casado, J.; López Navarrete, J. T.; Yu, X.; Facchetti, A.; Marks, T. J. Alkoxy-Functionalized Thienyl-Vinylene Polymers for Field-Effect Transistors and All-Polymer Solar Cells. *Adv. Funct. Mater.* **2014**, *24*, 2782−2793.
(22) Huang, H.; Chen, Z.; Ponce Ortiz, R.; Newman, C.; Usta, H.; Lou, S.; Youn, J.; Noh, Y. Y.; Baeg, K. J.; Chen, L. X.; Facchetti, A.; Marks, T. J. Combining Electron-Neutral Building Blocks with Intramolecular "Conformational Locks" Affords Stable, High-Mobility p- and n-Channel Polymer Semiconductors. *J. Am. Chem. Soc.* **2012**, *134*, 10966−10973.
(23) Do, K.; Saleem, Q.; Ravva, M. K.; Cruciani, F.; Kan, Z.; Wolf, J.; Hansen, M. R.; Beaujuge, P. M.; Bredas, J. L. Impact of Fluorine Substituents on π-Conjugated Polymer Main-Chain Conformations, Packing, and Electronic Couplings. *Adv. Mater.* **2016**, *28*, 8197−8205.
(24) Nielsen, C. B.; White, A. J.; McCulloch, I. Effect of Fluorination of 2,1,3-Benzothiadiazole. *J. Org. Chem.* **2015**, *80*, 5045−5048.
(25) Wang, Y.; Parkin, S. R.; Gierschner, J.; Watson, M. D. Highly Fluorinated Benzobisbenzothiophenes. *Org. Lett.* **2008**, *10*, 3307−3310.
(26) Chen, Z.; Cai, P.; Chen, J.; Liu, X.; Zhang, L.; Lan, L.; Peng, J.; Ma, Y.; Cao, Y. Low Band-Gap Conjugated Polymers with Strong Interchain Aggregation and Very High Hole Mobility Towards Highly Efficient Thick-Film Polymer Solar Cells. *Adv. Mater.* **2014**, *26*, 2586−2591.
(27) Zhou, X.; Ai, N.; Guo, Z.-H.; Zhuang, F.-D.; Jiang, Y.-S.; Wang, J.-Y.; Pei, J. Balanced Ambipolar Organic Thin-Film Transistors Operated under Ambient Conditions: Role of the Donor Moiety in Bdopv-Based Conjugated Copolymers. *Chem. Mater.* **2015**, *27*, 1815−1820.
(28) Zhao, K.; Ye, L.; Zhao, W.; Zhang, S.; Yao, H.; Xu, B.; Sun, M.; Hou, J. Enhanced Efficiency of Polymer Photovoltaic Cells Via the Incorporation of a Water-Soluble Naphthalene Diimide Derivative as a Cathode Interlayer. *J. Mater. Chem. C* **2015**, *3*, 9565−9571.
(29) Zhao, W.; Ye, L.; Zhang, S.; Yao, H.; Sun, M.; Hou, J. An Easily Accessible Cathode Buffer Layer for Achieving Multiple High Performance Polymer Photovoltaic Cells. *J. Phys. Chem. C* **2015**, *119*, 27322−27329.
(30) Zhao, W.; Ye, L.; Zhang, S.; Fan, B.; Sun, M.; Hou, J. Ultrathin Polyaniline-Based Buffer Layer for Highly Efficient Polymer Solar Cells with Wide Applicability. *Sci. Rep.* **2014**, *4*, 6570.
(31) Guo, X.; Zhang, M.; Ma, W.; Ye, L.; Zhang, S.; Liu, S.; Ade, H.; Huang, F.; Hou, J. Enhanced Photovoltaic Performance by Modulating Surface Composition in Bulk Heterojunction Polymer Solar Cells Based on PBDTTT-C-T/PC_{71} BM. *Adv. Mater.* **2014**, *26*, 4043−4049.
(32) Zhang, K.; Zhong, C.; Liu, S.; Mu, C.; Li, Z.; Yan, H.; Huang, F.; Cao, Y. Highly Efficient Inverted Polymer Solar Cells Based on a Cross-Linkable Water-/Alcohol-Soluble Conjugated Polymer Interlayer. *ACS Appl. Mater. Interfaces* **2014**, *6*, 10429−10435.
(33) Zhong, C.; Liu, S.; Huang, F.; Wu, H.; Cao, Y. Highly Efficient Electron Injection from Indium Tin Oxide/Cross-Linkable Amino-Functionalized Polyfluorene Interface in Inverted Organic Light Emitting Devices. *Chem. Mater.* **2011**, *23*, 4870−4876.
(34) He, Z.; Xiao, B.; Liu, F.; Wu, H.; Yang, Y.; Xiao, S.; Wang, C.; Russell, T. P.; Cao, Y. Single-Junction Polymer Solar Cells with High Efficiency and Photovoltage. *Nat. Photonics* **2015**, *9*, 174−179.

DOI: 10.1021/acsami.6b11348
ACS Appl. Mater. Interfaces 2016, 8, 31348−31358